

Cite this: *Soft Matter*, 2012, **8**, 3058

www.rsc.org/softmatter

COMMUNICATION

Role of disclinations in determining the morphology of deformable fluid interfaces†

N. Ramakrishnan,^{*a} John H. Ipsen^{*b} and P. B. Sunil Kumar^{*ab}

Received 15th December 2011, Accepted 30th January 2012

DOI: 10.1039/c2sm07384f

We study the equilibrium shapes of vesicles, with an in-plane nematic order, using a Monte-Carlo scheme and show that highly curved shapes, like tubes and discs, with a striking similarity to the structures engendered by certain curvature sensing peripheral membrane proteins, can be spontaneously generated by anisotropic directional curvature with nematic disclinations playing an important role. We show that the coupling between nematic order and local curvature could lead to like defects moving towards each other and unlike defects moving away, in turn leading to tube formation. Thermally induced defect pair production lead to branched tubular structures. It is also shown that a helical arrangement of the membrane tubes, with nematic field spiraling around it, is the dominant soft mode of the system.

Fluid interfaces with an in-plane orientational order can sustain amazingly complex morphologies. Apart from the interesting physics that it can offer, in terms of disclination dynamics on deformable surfaces, study of such interfaces also contributes to understanding the morphologies of cellular organelles.

The organelles of a biological cell have membranes with highly curved edges and tubes, as seen in the endoplasmic reticulum, the Golgi and the inner membrane of mitochondria. Tubulation has also been observed, *in vitro*, in self assembled systems of pure lipids.¹ It has been shown that macromolecules, which constitute and decorate the membrane surface, strongly influence the morphology of membranes. For instance proteins from the dynamin superfamily are known to pull out membrane tubes while oligomerizing themselves into a helical coat along the tube.² The BAR domain containing proteins can, in general, induce a wide spectrum of membrane shapes ranging from protrusions to invaginations depending on the geometry and interaction strength of the BAR domain.^{3–5}

The standard Helfrich model⁶ for membranes, based on mean curvature energy, cannot explain the stability of such highly curved structures. Existence of anisotropic bending energy will be the minimal requirement to explain the stability of tubular shapes, which

could arise from an in-plane orientational field on the membrane.^{7,8} Planar orientational order could be intrinsic to the membrane,⁹ due to the structural properties of its constituents, or could arise as a result of membrane interactions with external agents.^{3–5} Lipid molecules tilted with respect to the layer normal, as seen in the L'_β ¹⁰ and P'_β ¹¹ phases, is a well known case of intrinsic in-plane orientational order. Anisotropic peripheral proteins (*curvactants*), inducing membrane deformations¹² either by scaffolding or by insertion of their amphipathic helices into the membrane,³ are examples for extrinsic sources of orientational order. In general the order can be represented by a *p*-atic surface field, invariant under rotations by $2\pi/p$. Equilibrium shapes of a surface with *p*-atic in-plane order, have been investigated earlier.^{13,14} Mean field phenomenological models of orientation order on membrane surfaces, in the context of lipid tilt and chirality, have predicted the stability of tubular membranes and helical ribbons.^{15–18} More recently, a mesoscopic particle model was used to show that presence of BAR domains on membrane surfaces can lead to tubulation and vesiculation.^{19,20}

The coupling of curvature to orientational order leads to interesting defect dynamics and thermally excited shapes. Thus in addition to its biological relevance, membranes with in plane order also provide a unique medium to study disclination dynamics on deformable surfaces. So far such studies have been carried out only on surfaces with prescribed curvature.²¹ Apart from the interesting physics that it can generate these investigations may also provide new routes to new functional materials.²²

In this paper we use the Monte Carlo model developed by us^{23,24} to explore the spectrum of vesicle shapes engendered by an in-plane nematic field \hat{m} . The technique developed by us enables one to go beyond the mean field regime and also to explore the full nonlinear regime. We scale all energies by $k_B T$. A moderate mean curvature stiffness $\kappa = 10$ is chosen to enable study of thermally induced shape fluctuations. Higher values of κ are chosen to study equilibrium shapes in the absence of thermal fluctuations. We choose the directional curvature moduli, along and perpendicular to the orientational field, as $\kappa_{||} = 5$ and $\kappa_{\perp} = 0$ respectively. The results with $\kappa_{\perp} \neq 0$ are qualitatively the same and are not discussed separately. We vary the spontaneous curvature along the in-plane field C_0 , to explore different shapes. The in-plane nematic field, distributed uniformly over the entire surface, is constrained to be in the ordered phase by setting the Lebwohl Lasher coupling constant $\epsilon_{LL} = 3k_B T$.²⁵ For this values of the coupling constant, with $\kappa_{||} = 0$, the nematic field orients itself on a tetrahedron with four $+1/2$ disclinations, as predicted in

^aDepartment of Physics, Indian Institute of Technology Madras, Chennai, 600036, India. E-mail: ram@physics.iitm.ac.in; sunil@physics.iitm.ac.in

^bMEMPHYS Center for Biomembrane Physics, University of Southern Denmark, Odense, DK, 5230, Denmark. E-mail: ipsen@memphys.sdu.dk

† Electronic supplementary information (ESI) available. See DOI: 10.1039/c2sm07384f

ref. 13. We will first investigate the effect of the directional spontaneous curvature on the equilibrium membrane conformations when the κ value is high so that thermal undulations can be neglected.

At high κ thermal undulation does not change the vesicle's shapes significantly and the shapes obtained from the equilibrium simulations will be the same as that from a mean field calculation. It is known that dynamic triangulation Monte Carlo (DTMC) models, based on the Helfrich Hamiltonian,⁶ do reproduce the mean field phase diagram of vesicles.²⁶ Here we determine the equilibrium shapes of decorated vesicles with an in-plane orientational order, also taking thermal fluctuations into account. As can be seen from Fig. 1, we see tubular and disc like shapes emerging, even when there are no constraints on the area to volume ratio of the vesicle. Directional spontaneous curvature and interaction between the disclinations are two important factors that determine the shape of these decorated vesicles. Since the membrane is self avoiding the constraint imposed by the fixed topology also plays a role.

Four curvatures can be identified, the curvatures along the principal directions c_1 , c_2 with $c_1 > c_2$ and the directional curvatures, c^\parallel , c^\perp , along and perpendicular to \hat{m} . Fig. 2 shows the distribution $P(c_i)$, of $c_i = 1, 2$, on a vesicle, for different C_0^\parallel values when $\kappa_\perp = 0$. It is clear from Fig. 2(a) and (b) that for $C_0^\parallel > 0$ the distributions have a single peak, with $P(c_1)$ peaking close to, but less than, the value of C_0^\parallel , while $P(c_2)$ peaks at zero. The resultant value of the principal curvature arising from the competition between the resistance to bending imposed by κ and the directional spontaneous curvature set by C_0^\parallel , is shown in Fig. 3. When κ decreases the peak position of $P(c_1)$ moves toward that of C_0^\parallel and then to a value higher than C_0^\parallel for $\kappa \sim 0$. Note that for $\kappa = 0$ there are no competing elastic forces and the desired directional curvature can be achieved by setting \hat{m} at an angle $\varphi \neq 0$ with respect to the direction of c_1 . For a tube, a non zero value of φ implies a configuration with nematic spiraling around the tube. The angle φ is shown in the inset of Fig. 3. As expected this angle is a decreasing function of the bending modulus κ and saturates to zero for large bending rigidity.

Negative spontaneous directional curvature ($C_0^\parallel < 0$) induces tubes to form into the vesicle. However, restrictions imposed by the membrane self avoidance and topology prevent a complete inversion of the membrane through inward tubulation. This leads to a bimodal

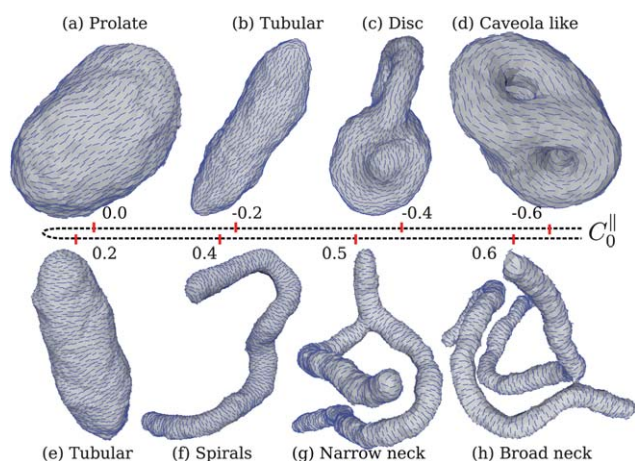


Fig. 1 Membrane conformations for different values of C_0^\parallel with $\kappa = 10$, $\kappa_\parallel = 5$, $\kappa_\perp = 0$ and $\varepsilon_{LL} = 3$. (See ESI for high resolution figures of nematic field arrangement†.)

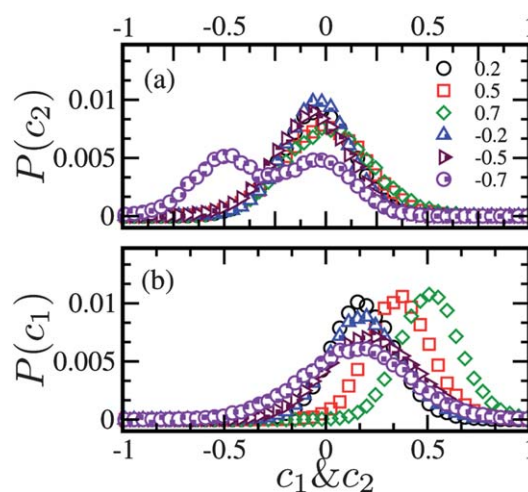


Fig. 2 (a,b) Distribution of the maximum and minimum principal curvatures, c_1 and c_2 respectively, for different values of C_0^\parallel .

distribution of c_2 , with a peak at $c_2 = 0$ in addition to the expected peak at $c_2 \approx C_0^\parallel$ (see Fig. 2(a)). This bimodal peak arises due to presence of inward tubes (with most of the vertices with $c_2 < 0$, $c_1 = 0$) and an outward curved surface (with most vertices having $c_1 > 0$, $c_2 = 0$).

Another important factor that determines the shape of a vesicle is the positioning of disclinations. We know that, for a nematic field on a closed surface with spherical topology, the total disclination strength should be 2. There is no such topological restriction on the number of defects themselves and thermal fluctuation could excite oppositely charged defect pairs.

In the absence of any stiffness-orientation coupling, the energy of a pair of defects, on a surface of spherical topology, decreases logarithmically with separation²⁷ and is repulsive when their charges are of the same sign.¹³ We therefore expect, at low temperatures, to see four $+1/2$ disclinations at equal distances from each other. In Fig. 4 evidence for this is shown in the single peak in the measured distribution of geodesic distances ($P(\xi)$) between the defects. Directional bending stiffness ($\kappa_\parallel \neq 0$) alters this distribution considerably, since curvature influences the interaction between defects.^{28,29} We see that two of the $+1/2$ defects move towards each other to form pairs as the vesicle deforms into a tube, resulting in a peak in the ξ distribution at

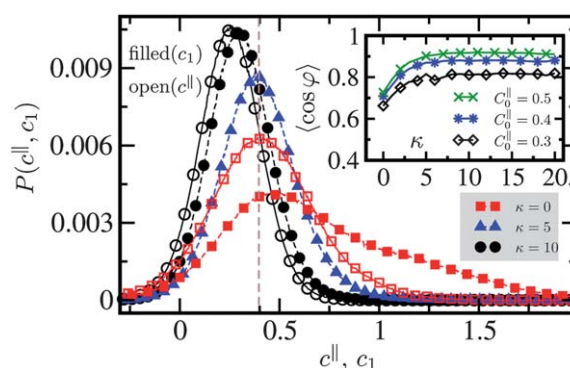


Fig. 3 Comparison of the c_1 (filled symbols) and directional curvature c^\parallel (open symbols) distribution, at $C_0^\parallel = 0.4$, $\kappa_\perp = 0$, for different values of κ . Inset shows the change in the angle φ as a function of κ . Dotted vertical line marks $c_1 = C_0^\parallel = 0.4$.

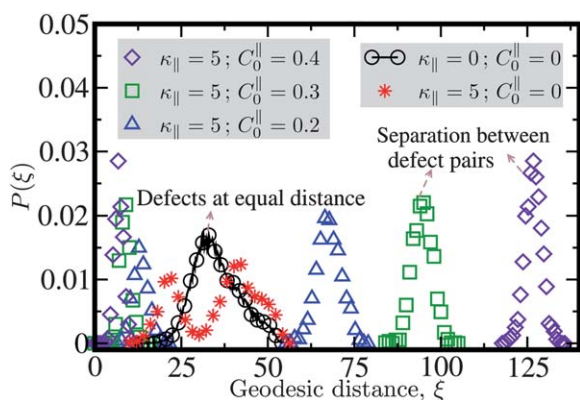


Fig. 4 Distribution of the nematic defect separation (ξ) for $\kappa = 10$, $\varepsilon_{LL} = 3$ and $\kappa_{\perp} = 0$.

short separation as shown in Fig. 4. This peak moves towards the left as C_0^{\parallel} increases. The pairs, which now has a total strength of +1, move away from each other, resulting in a second peak in $P(\xi)$. This peak position moves to the right as C_0^{\parallel} is increased. We thus observe nontrivial changes in the interaction between disclinations due to the geometry of the embedding surface. For $C_0^{\parallel} < 0$, there is a proliferation of defects as the inward tubes are formed. The inner side of the tubes are decorated with \hat{m} along the circumference with the tip hosting a pair of +1/2 defects. There is a sudden change in the orientation of \hat{m} just outside the rim of the tube (see Fig. 5). The rim itself is thus a line of discontinuity. There are two types of rims, closed ones with four -1/2 defects outside and paired open rims ending in two -1/2 defects.

A variety of thermally excited shapes are also seen. The lowest energy thermal modes among the tubes are the spirals, which are always present unless one is at a very low temperature (see Fig. 1(f)). If we raise the temperature or decrease the value of ε_{LL} , the tubes develop branches. More branches are produced as the temperature is increased, with every branch having a pair of -1/2 defects at the intersection and a pair of +1/2 defects at the tip.²⁴ Fig. 6 shows the sequence of snap shots that depict the transformation of a sphere with an initial random orientation of the nematic to a tube, when quenched from $\varepsilon_{LL} = 0$ to $\varepsilon_{LL} = 3$, while keeping $\kappa_{\parallel} = 5$, $\kappa_{\perp} = 0.0$, $\kappa = 10$ and $C_0^{\parallel} = 0.4$.³⁰ The nematic instantly orients on the sphere

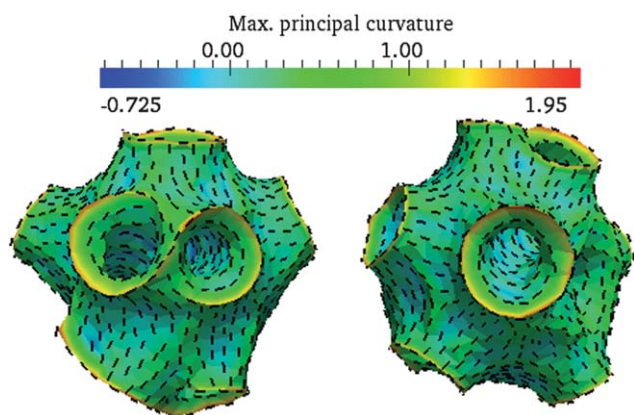


Fig. 5 Line discontinuities in the nematic orientation for $C_0^{\parallel} < 0$. (a) Paired tubes have rims that end on -1/2 defects while closed rims are surrounded by four -1/2 defects (b).

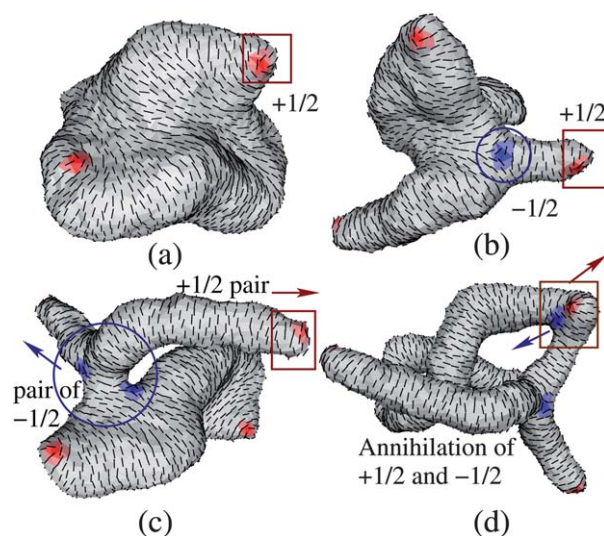


Fig. 6 The formation of tubes and branches are driven by proliferation of a +1/2 and -1/2 defect pairs. See text for details.

resulting in four +1/2 defects at equal distance from each other. The membrane then begins to deform, through formation of protrusions at the defect cores (Fig. 6(a)), since positive defects favor positively curved regions²⁸ and to satisfy the curvature set by C_0^{\parallel} and κ . These membrane protrusions are accompanied by the production of oppositely charged half defect pairs (Fig. 6(b)). The negative defects move to the negatively curved intersections and the positive defects move to the positively curved tip of the protrusions. When the tip of a protrusion has two +1/2 defects, and its neck two -1/2, that branch is stabilized and grows by moving the positive and negative defect pairs away from each other (Fig. 6(c)). Isolated +1/2 and -1/2 defects annihilate (Fig. 6(d)). In general two types of branched structures are observed, as we increase the directional spontaneous curvature, (a) *broad necked*, see Fig. 1(g) and (b) *narrow necked*, see Fig. 1(h).

To analyze the origin of helicity, we neglect the end cap effects of the tube and parameterize it as a *canal surface*. The total elastic energy, per unit length, is then,²⁴

$$H_{\text{tot}} = \frac{\pi}{r} \left(\varepsilon_{LL} \left(1 - \sqrt{1 - (\lambda r)^2} \right) + \left(\frac{\kappa + \kappa_{\parallel} (1 - x)^2 + \kappa_{\perp} x^2}{\sqrt{1 - (\lambda r)^2}} \right) + \left(\frac{\kappa_{\parallel}}{2} (1 - C_0^{\parallel} r) \right) (2x - 1 - H C_0^{\parallel} r) + \frac{\kappa_{\perp}}{2} (1 - C_0^{\perp} r) (1 - 2x - C_0^{\perp} r) \right).$$

Here r is the radius of the tube and $x = \cos^2 \varphi$. The energy depends only on the curvature of its spine curve λ , and not on the torsion, hence for $\lambda \neq 0$ there is a degeneracy of spiral configurations corresponding to different torsions. One can easily see that the energy is at its minimum when $\lambda = 0$.²⁴ For a tube of length L , parametrizing the spiral deformations by the extension of the tube along the helical axis $L_z = L\sqrt{1 - \lambda r}$, we can estimate the entropy to be of the order $k_B T \ln \left(\frac{L}{a} \right)$ and for small λ values the entropy term will dominate the free energy resulting in helical configurations.

Before we conclude, let us look at how the model parameters like the spontaneous curvature and the density of nematic inclusions compare with experiments. For $C_0 \sim 1.0$, the circumference of the tube is about 4 tether lengths. Comparing this with the radius of the lipid tubes obtained in experiments³¹ we get the length of the tether to be $\approx 25\text{nm}$. The value of $C_0 = 1.0$ in real units is thus $\approx (25\text{ nm})^{-1}$, which is not far from the suggested value of dynamin intrinsic curvature. Experiments see the dynamin rings surrounding the tubes to be made of about 20 units with a pitch of about 15 nm. This will translate to about 5 dynamin molecules per vertex in the simulations.

In conclusion, we have shown that in-plane nematic order coupled to curvature, on a deformable surface, can lead to non-trivial shapes of vesicles. The deformability of the surface lead to generation of point defects and line singularities, which in turn leads to production of tubes and branches.

References

- 1 M. Markowitz and A. Singh, *Langmuir*, 1991, **7**, 16–18.
- 2 G. J. K. Praefcke and H. T. McMahon, *Nat. Rev. Mol. Cell Biol.*, 2004, **5**, 133–47.
- 3 J. Zimmerberg and M. M. Kozlov, *Nat. Rev. Mol. Cell Biol.*, 2006, **7**, 9–19.
- 4 G. K. Voeltz and W. A. Prinz, *Nat. Rev. Mol. Cell Biol.*, 2007, **8**, 258–64.
- 5 Y. Shibata, J. Hu, M. M. Kozlov and T. A. Rapoport, *Annu. Rev. Cell Dev. Biol.*, 2009, **25**, 329–54.
- 6 W. Helfrich, *Z. Naturforsch. C*, 1973, **28**, 693.
- 7 J. B. Fournier, *Phys. Rev. Lett.*, 1996, **76**, 4436–4439.
- 8 J.-B. Fournier and P. Galatola, *Brazilian J. Phys.*, 1998, **28**, 329.
- 9 V. Kralj-Iglic, B. Babnik, D. R. Gauger, S. May and A. Iglic, *J. Stat. Phys.*, 2006, **125**, 727.
- 10 G. S. Smith, E. B. Sirota, C. R. Safinya and N. A. Clark, *Phys. Rev. Lett.*, 1988, **60**, 813.
- 11 A. Tardieu, V. Luzzati and F. C. Reman, *J. Mol. Biol.*, 1973, **75**, 711–718.
- 12 Y. Yin, A. Arkhipov and K. Schulten, *Structure*, 2009, **17**, 882–892.
- 13 J. Park, T. C. Lubensky and F. C. MacKintosh, *Europhys. Lett.*, 1992, **20**, 279.
- 14 F. C. MacKintosh and T. C. Lubensky, *Phys. Rev. Lett.*, 1991, **67**, 1169–1172.
- 15 W. Helfrich and J. Prost, *Phys. Rev. A: At., Mol., Opt. Phys.*, 1988, **38**, 3065.
- 16 P. Nelson and T. Powers, *Phys. Rev. Lett.*, 1992, **69**, 3409–3412.
- 17 J. V. Selinger and J. M. Schnur, *Phys. Rev. Lett.*, 1993, **71**, 4091.
- 18 J. M. Schnur, *Science*, 1993, **262**, 1669–76.
- 19 G. S. Ayton, P. D. Blood and G. A. Voth, *Biophys. J.*, 2007, **92**, 3595.
- 20 G. S. Ayton, E. Lyman, V. Krishna, R. D. Swenson, C. Mim, V. M. Unger and G. A. Voth, *Biophys. J.*, 2009, **97**, 1616.
- 21 H. Shin, M. Bowick and X. Xing, *Phys. Rev. Lett.*, 2008, **101**, 037802.
- 22 D. R. Nelson, *Nano Lett.*, 2002, **2**, 1125–1129.
- 23 N. Ramakrishnan, P. B. S. Kumar and J. H. Ipsen, *Phys. Rev. E: Stat., Nonlinear, Soft Matter Phys.*, 2010, **81**, 41922.
- 24 See ESI†.
- 25 P. A. Lebowitz and G. Lasher, *Phys. Rev. A: At., Mol., Opt. Phys.*, 1972, **6**, 426.
- 26 G. Gompper and D. M. Kroll, *Phys. Rev. Lett.*, 1994, **73**, 2139.
- 27 T. C. Lubensky and J. Prost, *J. Phys. II*, 1992, **2**, 371–382.
- 28 M. Bowick and L. Giomi, *Adv. Phys.*, 2009, **58**, 449.
- 29 V. Vitelli and D. R. Nelson, *Phys. Rev. E: Stat., Nonlinear, Soft Matter Phys.*, 2006, **74**, 21711.
- 30 Such a quench can be achieved by a change in temperature across the isotropic–nematic transition, wherein the mean bending modulus remains almost the same but there is a sharp change in the nematic stiffness.
- 31 S. M. Sweitzer and J. E. Hinshaw, *Cell*, 1998, **93**, 1021–9.